Increase in Aerosol Black Carbon in the 2000s over Ny-Ålesund in the Summer

LIQI CHEN AND WEI LI

Key Laboratory of Global Change and Marine-Atmospheric Chemistry, Third Institute of Oceanography, State Oceanic Administration, Xiamen, China

JIANQIONG ZHAN

Key Laboratory of Global Change and Marine-Atmospheric Chemistry, Third Institute of Oceanography, State Oceanic Administration, Xiamen, and State Key Laboratory of Atmospheric Boundary Layer Physics and Atmospheric Chemistry (LAPC), Institute of Atmospheric Physics, Chinese Academy of Sciences, Beijing, China

JIANJUN WANG, YUANHUI ZHANG, AND XULIN YANG

Key Laboratory of Global Change and Marine-Atmospheric Chemistry, Third Institute of Oceanography, State Oceanic Administration, Xiamen, China

(Manuscript received 1 January 2015, in final form 15 August 2015)

ABSTRACT

To investigate the concentrations, sources, and temporal variations of atmospheric black carbon (BC) in the summer Arctic, routine ground-level observations of BC by optical absorption were made in the summer from 2005 to 2008 at the Chinese Arctic ''Yellow River'' Station (78°55′N, 11°56′E) at Ny-Ålesund on the island of Spitsbergen in the Svalbard Archipelago. Methods of the ensemble empirical-mode decomposition analysis and back-trajectory analysis were employed to assess temporal variation embedded in the BC datasets and airmass transport patterns. The 10th-percentile and median values of BC concentrations were 7.2 and 14.6 ng m^{-3}, respectively, and hourly average BC concentrations ranged from 2.5 to 54.6 ng m^{-3}. A gradual increase was found by 4 ng m^{-3} a^{-1}. This increase was not seen in the Zeppelin Station and it seemed to contrast with the prevalent conception of generally decreasing BC concentration since 1989 in the Arctic. Factors responsible for this increase such as changes in emissions and atmospheric transport were taken into consideration. The result indicated that BC from local emissions was mostly responsible for the observed increase from 2005 to 2008. BC temporal variation in the summer was controlled by the atmospheric circulation, which presented a significant 6–14-day variation and coherent with 1–3- and 2–5-day and longer cycle variation. Although the atmospheric circulation changes from 2005 to 2008, there was not a marked trend in long-range transportation of BC. This study suggested that local emissions might have significant implication for the regional radiative energy balance at Ny-Ålesund.

1. Introduction

Arctic temperatures have increased almost twice as much as the global average over the last 100 yr (Quinn et al. 2011). Black carbon (BC) is generated by anthropogenic combustion of fossil fuel (e.g., coal, oil, gasoline) and biofuel (e.g., wood for stoves and heating) and emissions from natural biomass burning (e.g., wildfires). BC is the most efficient atmospheric particulate species at absorbing visible light, which absorbs approximately 1 million times more solar energy than CO_2 per unit mass (Bond and Sun 2005). BC is considered a significant contributor to Arctic warming as it not only absorbs solar radiation and alters cloud formation (Bauer and Menon 2012) but also darkens snow and ice when deposited (IPCC 2013). Uncertainty still remains regarding the role of BC in climate change (Bond et al. 2013).

Spatial and temporal distribution and potential sources of BC have been conducted in the Arctic. Eleftheriadis et al. (2009) made measurements at Zeppelin, Ny-Ålesund on the island of Spitsbergen in the Svalbard Archipelago [474 m above mean sea level (MSL)], from 1998 to 2007,

Corresponding author address: Liqi Chen, Key Laboratory of Global Change and Marine-Atmospheric Chemistry, Third Institute of Oceanography, State Oceanic Administration, Xiamen Daxue Road, Xiamen, Fujian 361005, China.
E-mail: chenliqi@tio.org.cn

DOI: 10.1175/JAS-D-15-0009.1

© 2016 American Meteorological Society

and found annual-average and -median BC concentrations of 39 and 28 ng m^{-3}, respectively, mainly influenced by source regions in northern and central Russia. Polissar et al. (1999) explored the possible sources impacting the measurement site at Point Barrow (71.2°N, 156.3°W); the result revealed that high BC concentrations were associated with pollution sources located to the north or northwest of Alaska. Sharma et al. (2004) focused on long-term trends at Alert (82.5°N, 62.5°W) and demonstrated that decreases in emissions from the Union of Soviet Socialist Republics (USSR) were mostly responsible for the BC decrease from 1989 to 2002. Sharma et al. (2006) also reported updated BC datasets at both Point Barrow and Alert over the 15-yr period from 1989 to 2003, showing that the differences in trends between the two sites may be related to the North Atlantic Oscillation (NAO). The potential source regions for the two sites were different: Alert is usually under the influence of transport from Siberia and Europe, while Barrow showed influence from Siberian and Pacific–Asian transport. Pollutants from these geographical regions have declined since early 1990s owing to the decreased emissions in these source regions (Quinn et al. 2011); therefore, their contribution to the aerosol loading in the Arctic has declined as well (Hirdman et al. 2010). During the past decade, human emissions including emissions from shipping and aviation have increased in the summer (Vestreng et al. 2009). Stohl et al. (2013) suggested that gas flaring has increased and may contribute 50% of aerosol loading in the Arctic. The shipping emissions in the Arctic may increase black carbon by 50% in 2030 in the Arctic lower troposphere (Dalsøren et al. 2009). At the Ny-Ålesund settlement, equivalent black carbon concentrations increased by 45% (Eckhardt et al. 2013) and the total suspended particulate mass was tripled (Zhan et al. 2014) when cruise ships were present at the harbor of the Ny-Ålesund settlement. Under the influence of the human activities, equivalent black carbon concentrations were found higher at the Ny-Ålesund settlement site than the values observed at the sites outside of the settlement (Zhan and Gao 2014). Therefore, it is reasonable to expect the temporal variation of BC at the Arctic settlement can be different from the background stations observed at the high-elevation sites [Zeppelin Station, Svalbard (78.90°N, 11.88°E; 474 m MSL); Alert, Nunavut (82.46°N, 62.50°W; 210 m MSL); Summit, Greenland (72.58°N, 38.46°W; 3216 m MSL)] and the trends in these stations could not be taken as representative of the overall BC trends at the lower elevation. To get a better overall view on BC trends and effects, higher resolution of temporal and spatial distribution of BC concentrations is required in the Arctic.

In this study, we present and discuss the concentrations and temporal variations of atmospheric BC concentrations at the Ny-Ålesund settlement in the summer from 2005 to 2008. We find an increase in BC concentration in the 2000s and it is higher than the mean concentration of the 1980s. Factors such as emissions and atmospheric circulation are discussed in order to explain the observed increase. This study will provide valuable BC observations at the settlement site as regards the limited data available in the Arctic. This settlement measurement is of particular interest as it has been suggested to have higher aerosol concentrations (Eckhardt et al. 2013; Zhan and Gao 2014), and this station is located near the glaciers, which are vulnerable to human perturbation (e.g., additional BC deposition).

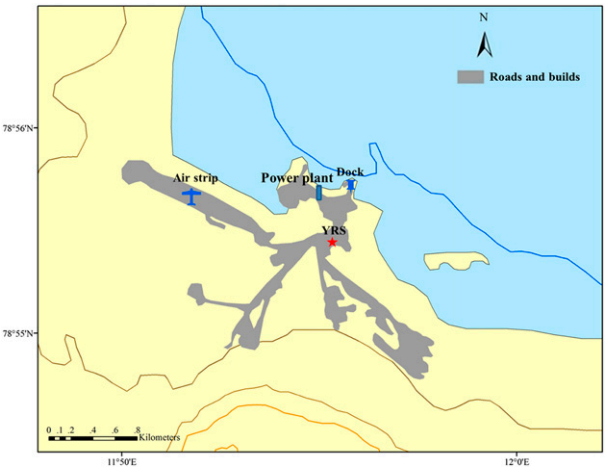

FIG. 1. Black carbon aerosol measuring site at the Yellow River Station (YRS), Ny-Ålesund.

2. Methods

a. *Sampling and measurement of aerosol black carbon*

The Chinese ''Yellow River'' Station (YRS) (see Fig. 1) is located at Ny-Ålesund. Pollution sources at the Ny-Ålesund settlement including ships, airplanes, and power stations may impact 1 km downwind of glaciated areas (Eckhardt et al. 2013; Zhan and Gao 2014). Continuous ground-based measurements of BC were made every summer from 2005 to 2008 at YRS using an aethalometer model AE-31 (seven wavelengths; only λ = 880 nm reported here; Magee Scientific, Berkeley, California). Temporal resolutions were 10 min during the measuring periods of 16 August–12 September 2005, 24 August–19 September 2006, 12 July–10 August 2007, and 25 July–12 August 2008. It determined the attenuation of light transmitted through particles that accumulate on a quartz fiber filter tape and interpreted the rate of increase of attenuation in terms of a

concentration of BC in the sampled airstream. The specific mass absorption coefficient $\alpha_{ap} = 15.9\,m^2\,g^{-1}$ was used to calculated BC mass concentrations, which was also applied in BC calculations at Zeppelin Station (Eleftheriadis et al. 2009). This value was derived from simultaneous measurements of light absorption and thermo-optical element carbon mass concentrations by Nyeki et al. (2005). The overall uncertainty on the aggregated data is on the order of 10% (Hansen et al. 2007). In this study, we use the abbreviation BC as we discuss black carbon in general and it is commonly used in the community.

b. Time series analysis

To determine both the dominate modes of variability and the variation of those modes with time in BC time series data, methods of the ensemble empirical-mode decomposition (EEMD) and Hilbert–Hung transform (HHT) analysis were employed to analyze it. As BC in nature is generated by nonlinear and nonstationary processes, a method of analysis should be adaptive to the nature of data. The EEMD method is a developed adaptive data analysis method, which has been used extensively in geophysical research (Huang and Wu 2008). This approach consists of sifting an ensemble of white-noise-added signal and obtains the mean of corresponding intrinsic-mode functions (IMFs) that bear the full physical meaning and a time–frequency distribution and also gets the corresponding average residual which is identical to the trend. Further details on the EEMD method can be found in Wu and Huang (2009).

Once the BC dataset is decomposed into a number of periodic components (IMFs) using the EEMD, the Hilbert transform is applied to each IMF, which was proposed by Huang et al. (1998, 1999) and Huang and Wu (2008). The Hilbert method provides time–frequency–energy distribution of time series data. Here, we give a brief description of the HHT; a detailed presentation can be found in the original articles of Huang et al. (1998, 1999). The Hilbert transform $y(t)$ of a function $x(t)$ is defined as $1/\pi$ times the convolution of f with the function $1/t$. Then, if $z(t)$ is the analytical signal, which can be formed with Hilbert transform pair using

$$z(t) = x(t) + iy(t) = A(t)\exp[i\theta(t)] \tag{1}$$

with

$$A(t) = [x_2(t) + y_2(t)]^{1/2} \quad \text{and} \quad \theta(t) = \arctan[y(t)x(t)]. \tag{2}$$

The instantaneous frequency can be written as the time derivative of the phase:

$$\omega(t) = \frac{d\theta(t)}{dt}. \tag{3}$$

Once the signal has been decomposed into IMFs and the Hilbert transform for each has been obtained, the signal $x(t)$ can be represented as

$$x(t) = \sum_{j=1}^{n} A_j(t)\exp\left[i\int \omega_j(t)\,dt\right], \tag{4}$$

which is a generalized form of the Fourier expansion for $x(t)$ in which both amplitude and frequency are functions of time. The time–frequency distribution of the amplitude or energy (square of amplitude) is defined as the Hilbert amplitude spectrum or the Hilbert energy spectrum, respectively.

In this study, the ensemble size for each dataset was set to 300; amplitude white noise of standard deviation = 0.3 was added to force the ensemble to exhaust all possible solutions in the sifting process. By this method, each dataset was decomposed into 300 groups of IMFs and then assembled into a finite and small number of IMFs, which represent various oscillations. HHT analysis was then performed using the method described in Huang et al. (1998). The results were tested by statistical significance in order to determine confidence levels.

c. Trajectory model and cluster analysis

The 7-day backward trajectories used in this analysis were simulated by the hybrid single-particle Lagrangian integrated trajectories (HYSPLIT) model (Draxler and Hess 1998) with $1^\circ \times 1^\circ$ resolution and a temporal resolution of 6 h. The model was run for 1000 m using 7-day back trajectories at 0000, 0600, 1200, and 1800 UTC. Cluster analysis was used to classify the trajectories into eight groups to separate pollution from different potential source regions.

3. Results and discussion

a. BC concentrations

The ranges of hourly BC concentrations are from a maximum of $54.6\,ng\,m^{-3}$ to a minimum of $2.5\,ng\,m^{-3}$, which is about one order of magnitude variation (see Fig. 2). The 10th-percentile value, showing the local background concentration, is $7.2\,ng\,m^{-3}$. This is comparable to measurements taken outside the Ny-Ålesund settlement in the summer of 2011, with a mean of $5.5\,ng\,m^{-3}$ (Zhan and Gao 2014), and is similar to that of Eleftheriadis et al. (2009), who reported a BC average concentration of $7\,ng\,m^{-3}$ at the Zeppelin Station during the summertime from 1998 to 2007. The median BC of

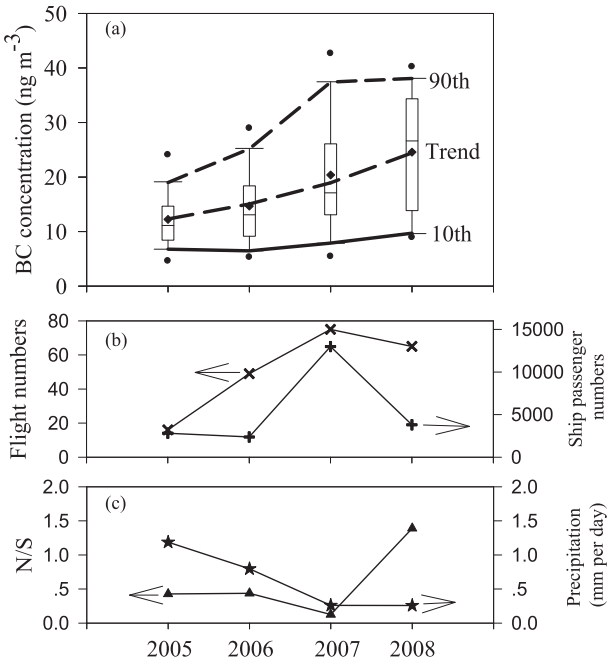

FIG. 2. (a) Box-and-whisker plot (median and 10th, 25th, 75th, and 90th percentiles) of BC at the Yellow River Station in the summertime from 2005 to 2008. Also shown are the mean (diamonds) and trend lines for the mean (long-dashed) and 90th (short-dashed) and 10th (solid) percentiles. (b) The number of flights (×) and ship passengers (+) for each sampling period. (c) The ratio of north wind to south wind (*N*/*S*; ▲) and precipitation (★).

our observation is 14 ng m^{-3}, which is similar to the median value (17 ng m^{-3}) observed at the same site in the summer of 2011 (Zhan and Gao 2014). The Zeppelin Station is at 474 m, while YRS is at sea level. As a ground-based station, YRS is more susceptive to local human activities, such as cruise ship tourism, station operations, and vessels (Eckhardt et al. 2013; Zhan and Gao 2014). As shown in Fig. 3, the north-corresponding BC concentrations were usually high. Since the residential area and quay lies northwest of the measuring station, high BC levels in the northern sector were most likely influenced by aerosols emitted from local human activities. However, residential sources would not explain all of the measured high BC concentration. High BC concentrations also appeared in the southern sector; this is in summer 2007. Several aspects should be taken into account, including changes in BC emissions and atmospheric circulation, which are discussed in the following sections.

The mean sea level BC concentration from the summer during 2005–08 at YRS is doubled, about 9 ng m^{-3} higher than those of Heintzenberg and Leck (1994), measured from 1979 to 1990 at the Gruvebadet sea level site with an elemental carbon concentration of 5 ng m^{-3} during the summer and autumn seasons. A clear feature of BC at YRS is the steady increase in BC concentrations of about 4 ng m^{-3} a^{-1} during the summertime from 2005 to 2008, as shown in Fig. 2. This increase is surprising as it contradicts the long-term trend measurement at Zeppelin, Alert, and Summit. A net decrease at both Alert and Barrow was observed during the 1990s (Sharma et al. 2006) and a declining trend of −9.5 ng m^{-3} decade^{-1} was found at Zeppelin from 2001 to 2007 for all yearly datasets (Eleftheriadis et al. 2009). A similar increase was found at Barrow during the summertime from about 1999 to 2002 (Sharma et al. 2006). The residential emissions were presumably a factor contributing to the observed increased trend at YRS. As shown in Fig. 1, these local emission sources were located north of the sampling site; thus, we employed the ratio of frequency of northwesterly wind to that of southeast (*N*/*S*), combined with precipitation and the number of flights and ships, to find out the variations that contributed to the BC concentration (see Figs. 2b and 2c). If we only compared these parameters for summer 2005, 2006, and 2008, the ratios of *N*/*S*, the number of flights and ships increased, and the precipitation decreased, the combined effect would lead to an increase in the BC concentration. Although, for the summer 2007, the number of flights and ships were highest and precipitation is lowest during the observation years, the *N*/*S* ratios were low—only 0.13—indicating the southerly prevailing wind; consequently, the pollutants generated in the north cannot efficiently reach the sampling site.

b. Time–frequency analysis for the BC concentrations

1) EEMD

To isolate and extract various temporal scales and trend embedding in the data, the time series of BC were analyzed using the EEMD method. The results are displayed in Fig. 4. The left panels show statistical significance testing and the right panels show that the original BC is decomposed into eight or nine components and one trend. The significance test shows all the other IMFs were statistically significant at 99% confidence levels. This suggests that periodicities ranging from 3 h to 15 days were found to be statistically significant in the BC dataset. Each IMF component represents the instantaneous amplitude features of the original signal in a different frequency range (the first IMF covers the highest frequencies and the last IMF covers the lowest one) and that each frequency band of the IMFs have crossovers with each other. These IMFs were used as regressors in the general linear model for BC, and the correlations between the IMFs and the

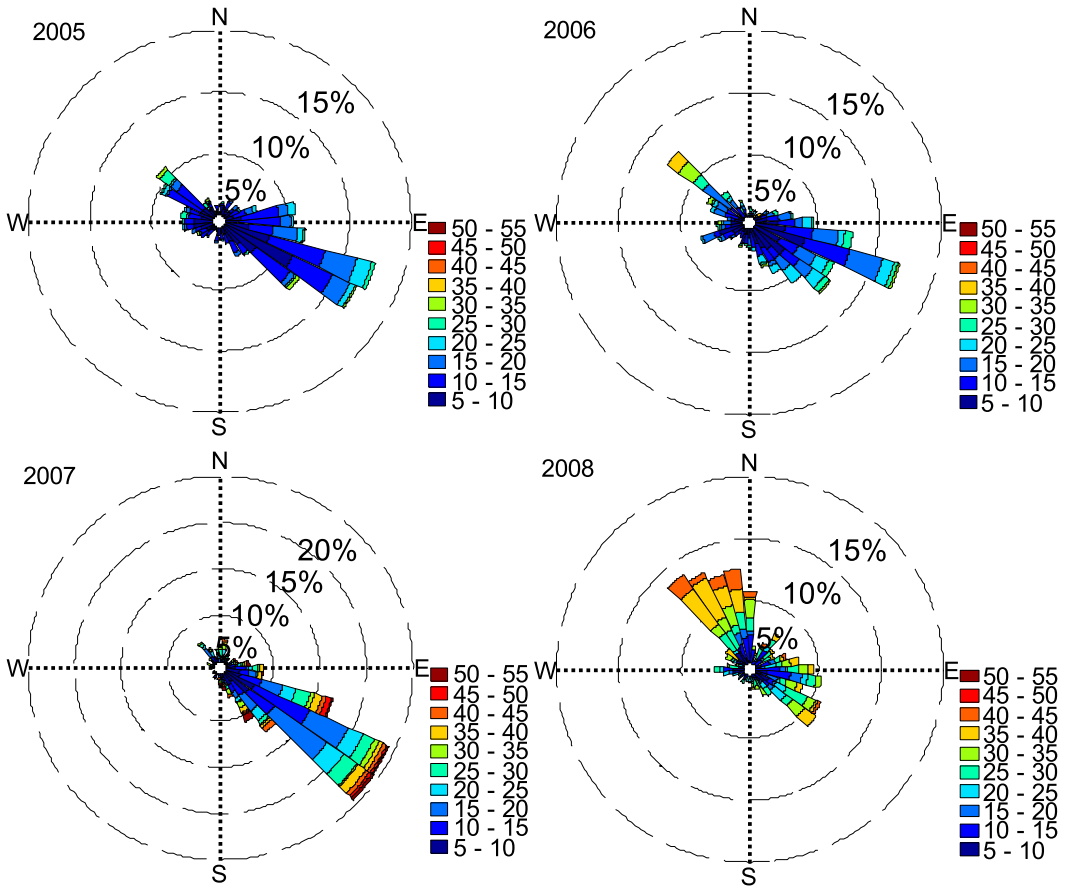

FIG. 3. Variations in black carbon concentration (ng m^{-3}) affected by wind directions at Yellow River Station. Individual wind direction measurements are accumulated and the relative frequency is shown as a percentage.

meteorological factors [e.g., wind speed (WS), temperature T, relative humidity (RH)] were used to explore the meteorological factors whose activity specifically correlated with each IMF.

For all data, IMF1 and IMF2 were mostly dominated by a component with periods of 2–5 and 6–12 h. There was low correlation between IMF1 or IMF2 and meteorological factors, with a Pearson correlation ranging from −0.036 to 0.044 ($p > 0.05$) (see Table 1), suggesting that local meteorological factors did not directly affect IMF1 and IMF2. The correlations between the other IMFs and meteorological elements were considerably different for each year. IMF3 presented a scale of a 0.5–2-day oscillation, of which the variation in 2005 and 2006 agreed well with RH, with a Pearson correlation of 0.170 ($p < 0.01$) and 0.101 ($0.01 < p < 0.05$), respectively. However, there was no significant correlation between them in 2007 and 2008, with a Pearson correlation of 0.020 ($p > 0.05$) and −0.023 ($p > 0.05$), respectively. IMF4 is mostly dominated by periods with 0.9–5.4 or 1–3 days. In 2005, when the NAO index was positive, IMF4 was represented by a variation of 0.9–5.4 days, which was correlated with wind speed ($r = 0.182$, $p < 0.01$). The 7-day back trajectories revealed that this variation was associated with the movement of low pressure systems across the North Atlantic, and then into the Arctic, with strong winds transporting pollutants from surrounding areas such as northern Europe. During the years of the negative NAO index (2006, 2007, and 2008), the back trajectory and IMFs showed that the dominant signal of a 1–3-day oscillation was associated with low pressure in Iceland. IMF5 had the frequency component of a 2–5-day variation, which showed significant positive correlation with WS (2005: $r = 0.166$, $p < 0.01$; 2006: $r = 0.282$, $p < 0.01$) and RH (2005: $r = 0.161$, $p < 0.01$; 2006: $r = 0.222$, $p < 0.01$) and negative correlation with T (2005: $r = -0.084$, $p < 0.01$; 2006: $r = -0.080$, $0.01 < p < 0.05$). This was associated with cold moist air masses transported by low pressure with strong winds from areas near Greenland and the movement of low pressure systems in the Arctic basin. However, in 2007 and 2008, this time-scale-factor

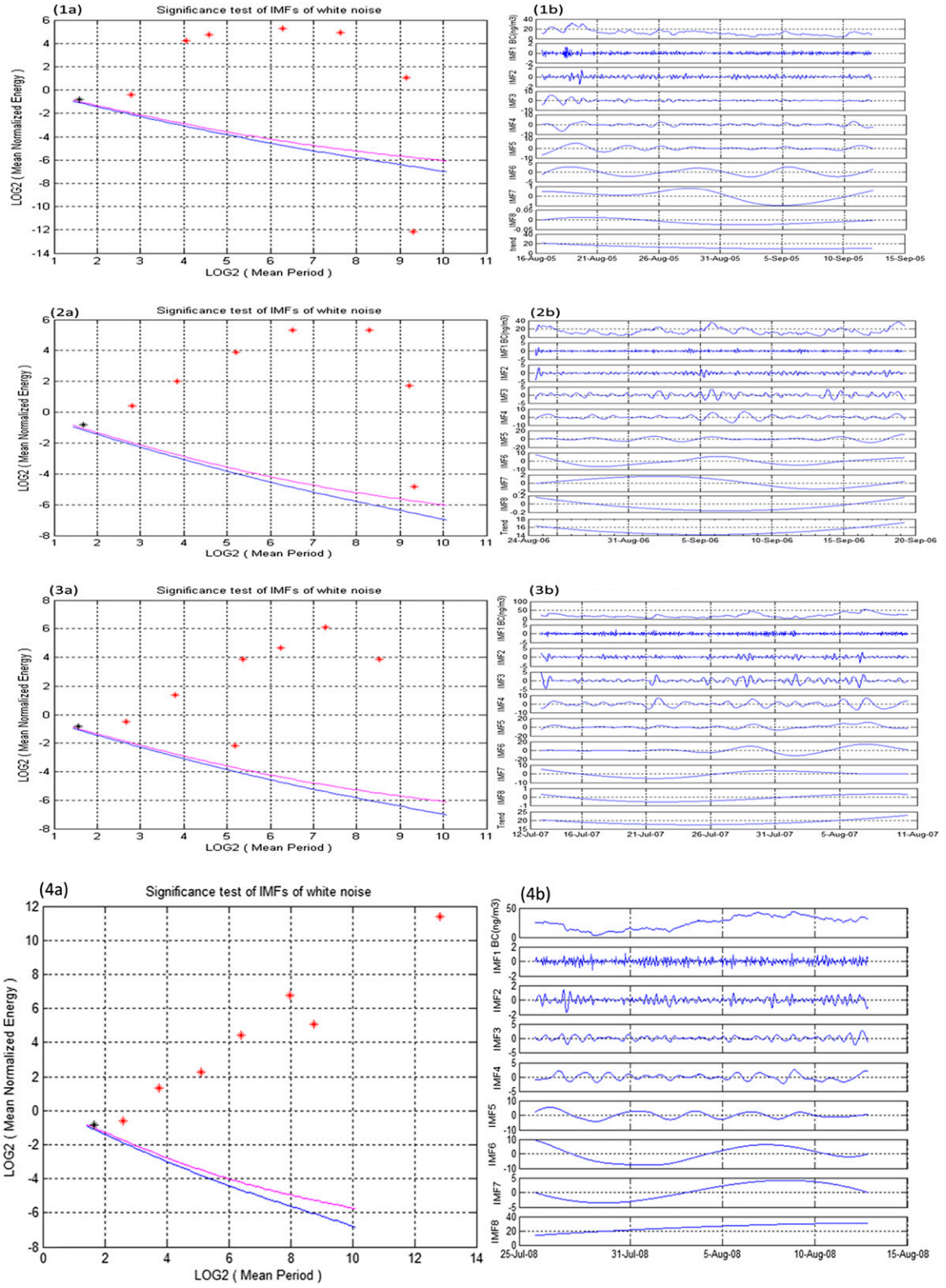

FIG. 4. (left) Log–log diagram of the energy and dominant period of the different intrinsic modes identified by the EEMD method and statistical significance test for IMFs of the BC concentration data with 95% (blue line) and 99% (pink line) confidence limit. Each asterisk below the lines indicates that the hypothesis that the corresponding IMF of the observed series is not distinguishable from the corresponding IMF of a random noise series cannot be rejected with the confidence levels (95% and 99%). (right) Time series of the BC concentrations and the extracted components (IMFs) and residual using the EEMD method.

TABLE 1. Correlation between IMFs and meteorological factors for the years from 2005 to 2008.

	IMF1	IMF2	IMF3	IMF4	IMF5	IMF6	IMF7	IMF8	IMF9
2005 (NAO^+)									
WS	0.017	0.037	0.018	0.182[a]	0.166[a]	0.015	0.237[a]	−0.101[b]	−0.248[a]
TEM	−0.028	0.006	−0.008	0.008	−0.084[b]	0.365[a]	0.186[a]	−0.163[a]	0.208[a]
RH	0.013	0	0.170[a]	−0.041	0.161[a]	−0.120[a]	0.124[a]	0.390[a]	0.417[a]
2006 (NAO^-)									
WS	0.037	0.044	−0.009	0.024	0.282[a]	−0.025	−0.219[a]	0.147[a]	0.270[a]
TEM	−0.036	−0.026	0.007	−0.084[b]	−0.080[b]	−0.391[a]	0.128[a]	−0.189[a]	−0.390[a]
RH	0.033	0.052	0.101[b]	0.068	0.222[a]	0.364[a]	0.387[a]	0.036	−0.106[a]
2007 (NAO^-)									
WS	0.013	0.015	−0.039	−0.011	0.048	0.006	−0.069	−0.006	0.002
TEM	−0.001	0.008	0.001	−0.034	0.198[a]	−0.110[a]	0.251[a]	0.201[a]	−0.012
RH	0.016	−0.007	0.028	0.02	−0.035	0.248[a]	0.03	0.127[a]	0.230[a]
2008 (NAO^-)									
WS	−0.003	0.02	0.108[b]	0.126[a]	−0.01	0.316[a]	0.159[a]	−0.023	—
TEM	−0.028	−0.014	0.021	0.059	0.274[a]	−0.108[b]	−0.597[a]	−0.705[a]	—
RH	0.028	0.029	−0.023	−0.047	−0.199[a]	−0.102[b]	0.253[a]	0.371[a]	—

[a] Correlation significant to the 99% confidence level (two tailed).
[b] Correlation significant to the 95% confidence level (two tailed).

variation had positive correlation with T (2007: $r = 0.198$, $p < 0.01$; 2008: $r = 0.274$, $p < 0.01$). This can be explained by activities of low pressure systems in Europe and northeastern Canada, which bring air masses from the continents of Europe and northeastern Greenland. IMF6 was mostly dominated by a frequency component of 6–14 days, except in 2007. The mean period of the IMF6 factor in 2007 was shorter, with a period of 3–8 days. In the NAO-positive-phase year of 2005, this oscillation showed positive correlation with T ($r = 0.365$, $p < 0.01$), while in the NAO-negative-phase year (2006–08), it showed negative correlation with T ($r = -0.391$, -0.110, and -0.108, $p < 0.05$). This indicated frequencies of North Atlantic cyclonic and Siberia cyclonic and activity, respectively, which could transport pollutants from North America and Eurasia. In short, in 2005 when the NAO index was positive, Ny-Ålesund was influenced more by low pressure system activity in the North Atlantic, which makes 0.9–5.4-day signals in the BC dataset. In NAO-negative-phase years, Aleutian low allows signals of low pressure systems in Europe and northeastern Canada and Siberia cyclonic activity to be more frequently included in the BC dataset.

2) HHT

We analyzed the Hilbert spectra for each IMF, which was decomposed from the BC dataset using the EEMD, where the energy level was given by a color scale (see Fig. 5). From this graph, it is possible to see a detailed record of the variation in frequency and energy with time. The normalized energies first increased and then decreased with the increase of period values. The distribution of energy is controlled by atmospheric circulation patterns. In 2005, energy tends to disperse and compress in IMF5, IMF6, IMF4, and IMF3, following, in decreasing order, variations of 6–14, 0.9–5.4, 2–5.4, and 0.5–2 days, respectively. In 2006, the energy peak values were between IMF5 and IMF6, with the variations of 5.4–15.5 and 2.5–5.2 days, respectively. The main periods in 2007 and 2008 were IMF6, followed by IMF5. Although the main period in 2007 and 2008 was IMF6, various scales were quite different; the energy peak in 2007 had a mean period of 6.5 days, which represented the variation range from 3 to 8 days, while in 2008 the peak was found to have a mean period of 9.6 days, which indicates a 6–14-day variation.

For all of the scaled data, the oscillations of 2–5 and 6–12 h and 0.5–2 days were random. Higher power of 1–3-day signals was found during 17–20 August, 26–27 August, and 10–11 September 2005; 5–8 and 18–19 September 2006; and 20–22 July, 29–30 July, and 4–9 August 2007. There were also 2–5-day ''oscillations'' in variance, especially prominent during 17–28 August and 8–12 September 2005, 29 August–6 September and 14–19 September 2006, and 29 July–8 August 2007. The period of 3–8 days was apparent during 25 July–10 August 2007. The oscillation of 6–14 days or longer was present all the time. The effects of particular scale will be explored and discussed in later sections.

c. *BC emissions*

The declined trend of the long-range transport of pollutants is well documented, which can be seen from the decrease of black carbon since the1990s (Hirdman et al. 2010; Sharma et al. 2013) due to the decreased source strengths since the 1990s (Quinn et al. 2011; Bond

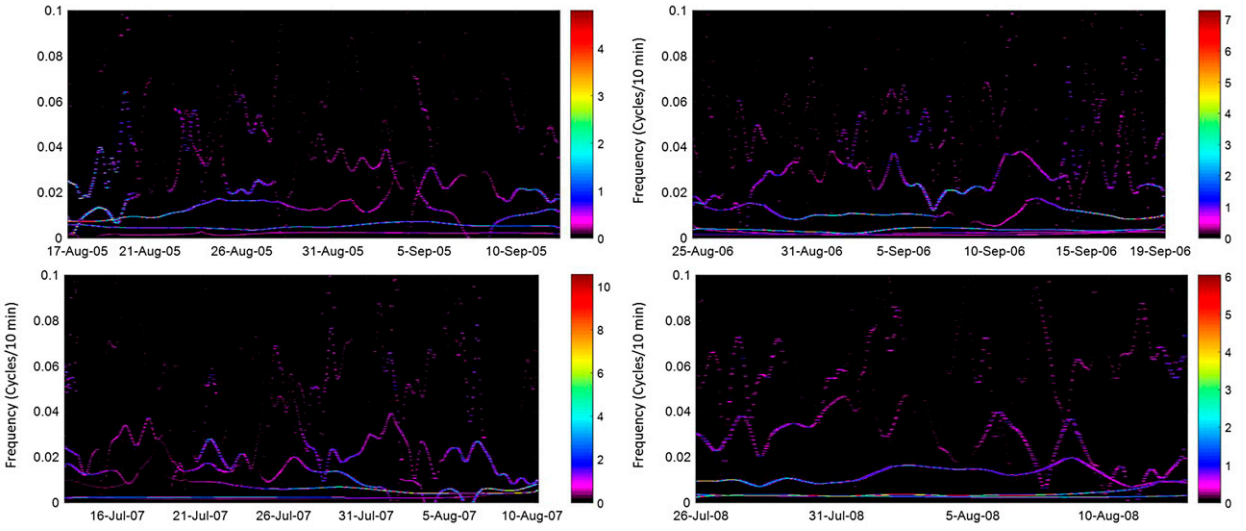

FIG. 5. Hilber–Huang spectrum of the BC concentration for the years of 2005, 2006, 2007, and 2008. The colors of the lines indicate the amplitude of the modes as a function of time. The form of the line represents the variation of the instantaneous period of the IMF as a function of time.

et al. 2013). Human activities such as oil and gas flaring, shipping, and exploitation have increased (Quinn et al. 2011), and therefore these sources are expected to be responsible for the increased BC concentration at Ny-Ålesund. The question is to what extent local emissions can explain the increase in BC concentration.

Here, EEMD method was employed to decompose time series of BC (BC_{total}) into various frequency signals, which are expressed as the IMFs and trend. The relation can be expressed as

$$BC_{total} = IMF_1 + IMF_2 + \cdots + IMF_n + Trend. \quad (5)$$

The BC concentrations at YRS are impacted by the local human activities and atmospheric circulation. We assumed background BC concentration (BC_{total}) at Ny-Ålesund was adjusted by the local emission (BC_{em}) and long-range transportation (BC_{tr}). So BC_{total} can be expressed as

$$BC_{total} = BC_{em} + BC_{tr}, \quad (6)$$

where BC_{em} is related to the random human activities and continuous emission. Random human activities are always included in the high-frequency signal and irrelevance with meteorological factors. Continuous emission can be included in the extreme low frequency signals $E_{low\text{-}em}$. It is defined as follows:

$$BC_{em} = IMF_1 + IMF_2 + \cdots + IMF_m + E_{low\text{-}em}. \quad (7)$$

The long-range transportation is determined by the atmospheric circulation that behaves various temporal scales of activities. They are

$$BC_{tr} = IMF_{m+1} + IMF_{m+2} + IMF_{m+3} + \cdots + IMF_n + E_{low\text{-}tr}, \quad (8)$$

where $E_{low\text{-}tr}$ is a longer variation of atmospheric circulation. For the principle of EEMD, residual (Trend) is representing longer oscillation, which includes the longer time scales of variation. Here it can be express as

$$Trend = E_{low\text{-}em} + E_{low\text{-}tr}. \quad (9)$$

In the calculations to follow, we first calculate the IMFs and the integrated functions given in Eqs. (5)–(9), and then we will obtain local emission (BC_{em}) and long-range transportation (BC_{tr}) (see Fig. 6). The results showed that only 34% of the BC is from local emission in 2005, and about half of the BC in 2006–08 is from local sources. BC_{em} increased from 2005 to 2008, about a rate of $3.7\,ng\,m^{-3}\,a^{-1}$. There is not a marked trend in BC_{tr}, with an increase from 2005 to 2006 and then a decrease from 2006 to 2008. Annual variability in transport paths and emission densities of BC leads to a considerable range in value of this contribution, which may reach 50% under conditions of very strong atmospheric transport. The results indicate that the rate of $4\,ng\,m^{-3}\,a^{-1}$ increase may be mainly due to changes in local emissions. It is worth noting that the highest BC_{tr} appeared in 2007, while from 2007 to 2008 mean of BC_{tr} deceased, which might be related to a global economic recession in 2008. It seems from the year 2005 and 2008, the overall contribution from long-range transport is variance, and how this atmospheric circulation regulating BC concentrations in the summer from 2005 to 2008 is discussed below.

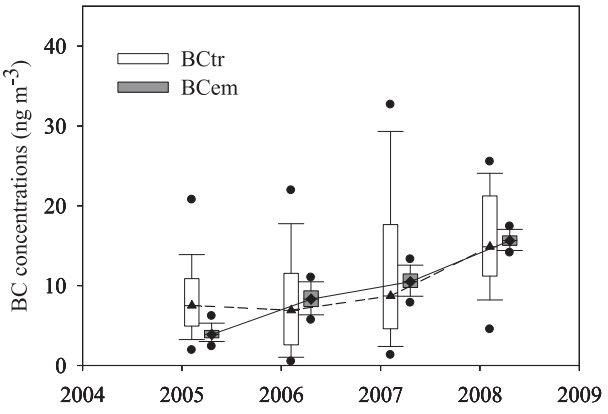

FIG. 6. Box-and-whisker plot of BC concentrations from local emissions (BC_{em}) and long-range transport (BC_{tr}) for each sampling period [median of BC_{em} (diamonds); mean of BC_{tr} (triangles); 10th, 25th, 50th, 75th, and 90th percentiles; and trend (solid line is BC_{em} and short dashed line is BC_{tr})].

d. Atmospheric circulation

Atmospheric circulation determines airmass origins, which determines the strength and transport en route of pollutants to the Arctic; therefore, atmospheric circulation has fingerprints in BC concentrations.

1) TRANSPORT PATHWAYS

The Yellow River Station at Svalbard in the community Ny-Ålesund was impacted by BC emission from various sources both the local human activities and outside transport. Atmospheric circulation patterns strongly influence the contribution of various source regions to the pollution in the Arctic. To identify the main pathways to the Yellow River Station in the Arctic, probability density plots for the 7-day back trajectories and the cluster analysis techniques were applied to the full dataset. The probability density functions for the Yellow River Station from 2005 to 2008 in summertime are displayed in Fig. 7. For the last 4 yr in summertime, eight potential source areas were identified as having potential contributions to BC at Yellow River Station. There are Baffin Bay–Canadian Archipelago (BB/CA; cluster 1), Bering Sea–Chukchi Sea–Beaufort Sea (BS/CS/BFS; cluster 2), East Siberian Sea–Eurasian basin (ESS; cluster 3), Laptev Sea–Kara Sea–Eurasian basin (LS/KS; cluster 4), Greenland–Greenland Sea (GL; cluster 5),Greenland Sea–Norwegian Sea (GS/NS; cluster 6), Scandinavia–Barents Sea–Kara Sea (SC/BS/KS; cluster 7), and Barents Sea (BS; cluster 8).

The variation of the frequency for each cluster is shown in Table 2. For all data, BS is dominant in terms of the frequency of back trajectories, about 47% from 2005 to 2007, while in 2008 the BS transport decreased because of increasing influence from the GL cluster. The result of prominent circulation patterns for Svalbard Islands agrees well with trajectories and cluster analysis at Zepplin (Eleftheriadis et al. 2009) and at Barrow and Alert studied by Sharma et al. (2006). Only occasionally, less than 2% of the trajectories are found in LS/KS (cluster 4). The average frequency of transport from other cluster range from 2.18% to 16.08%, followed in decreasing order by the GL (16.08%), SC/BS/KS (15.91%), ESS (8.40%), BS/CS/BFS (6.21%), BB/CAA (4.70%), and SC/BS/KS (2.81%). There were noticeable differences in frequency between the clusters year to year, pointing at different likely source areas. Previous studies (Eleftheriadis et al. 2009; Sharma et al. 2006) revealed that the NAO is a major indicator of one of the dominant sources of Northern Hemispheric circulation changes. To examine how atmospheric circulation pattern affected the clustering in summer, the frequency of trajectories for each year was compared with the corresponding NAO index. The results revealed that the relationship between NAO and the year-to-year frequency in summer was not clear, which may be because of insufficient data for statistics. So the mean of frequencies for positive and negative phases of NAO have been calculated separately. The result revealed that the frequency of trajectories transported from GS/NS was enhanced during the positive phase of NAO, while during the negative phase of NAO, the frequency decreased to only 0.58 in 2007. Svalbard Islands had a larger influence from the BS, GL, and GS/NS clusters, which transported pollution from northern Europe and the North Atlantic Ocean. The impact of the NAO phases on pollution and BC concentration will be investigated in the next section.

2) SOURCE CONTRIBUTIONS TO BC

In the summer, the pressure field is typically quite flat, and winds are light and variable. Pressures are actually lowest over the central Arctic Ocean, and weather patterns are dominated by the movement of low pressure systems across Siberia or the Atlantic Ocean into the Arctic basin with pollution transported from the periphery that is manifest as variations in BC. To strengthen the argument for the source contribution, we use variations in BC_{tr} (long-range transportation of BC) to investigate the main source regions. Here, we used BCA_{tr}, defined as BC_{tr} minus the median of BC_{tr}, to investigate the contribution of the each cluster to investigate the main sources. A box-and-whisker plot of BCA_{tr} from each cluster is shown in Fig. 8.

For all clusters in the years from 2005 to 2008, BCA_{tr} concentrations associated with the air mass

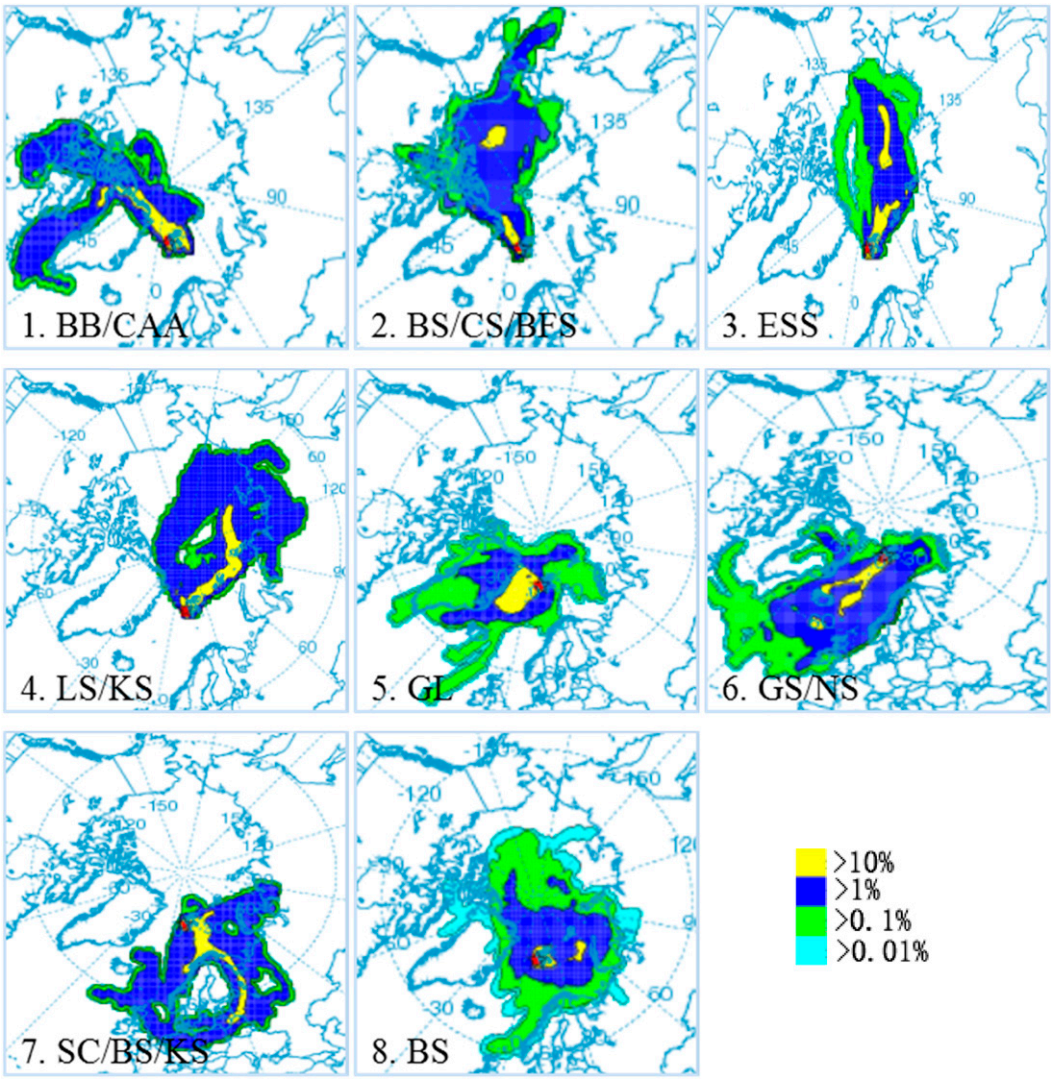

FIG. 7. Probability density functions of the 7-day back trajectories for each of pathways arriving at Yellow River Station from 2005 to 2008 in the summer. Eight pathways are defined as Baffin Bay–Canadian Archipelago (BB/CA; cluster 1), Bering Sea–Chukchi Sea–Beaufort Sea (BS/CS/BFS; cluster 2), East Siberian Sea–Eurasian basin (ESS; cluster 3), Laptev Sea–Kara Sea–Eurasian basin (LS/KS; cluster 4), Greenland–Greenland Sea (GL; cluster 5),Greenland Sea–Norwegian Sea (GS/NS; cluster 6), Scandinavia–Barents Sea–Kara Sea (SC/BS/KS; cluster 7), and Barents Sea (BS; cluster 8). The frequency of trajectories is indicated in the key: greater than or equal to 10% (yellow), greater than or equal to 1% and less than 10% (blue), greater than or equal to 0.1% and less than 1% (green), and greater than or equal to 0.01% and less than 0.1% (cyan).

from SC/BS/KS and GS/NS in 2007 were significantly higher than BCA_{tr} concentrations in all of the other clusters, with BCA_{tr} concentrations up to 16.8 and 22.3 ng m^{-3}, respectively. The variance of BCA_{tr} in the SC/BS/KS cluster was the most significant, as most of the trajectories in this cluster passed over strong source areas such as cities in Sweden, Finland, Russia, and Poland, long-range transport from which would bring pollutants to the station. Trajectories in the GS/NS cluster were from the Norwegian Sea and were long enough to transport air from the area of Scotland and Ireland to the sampling station from the south. The main mode pattern in the GS/NS cluster had a variation period of 2–5 days, while the SC/BS/KS cluster had a major variation period of 3–8 days. Transport of pollutants in the GS/NS cluster may be associated with Atlantic cyclones, while SC/BS/KS was affected by the impact of low pressure systems over the continent.

In comparison, the LS/KS cluster was relatively clean with $BCA_{tr} \leq 0$ ng m^{-3} because of greater scavenging

TABLE 2. The frequency of trajectories for each cluster at Ny-Ålesund in the summer months from 2005 to 2008.

Year	BB/CAA	BS/CS/BS	ESS	LS/KS	GL	GS/NS	SC/BS/KS	BS	NAO index
2005	2.79	5.43	—	1.09	6.67	36.43	0.62	46.98	0.5
2006	—	3.23	—	1.29	27.9	19.03	—	48.55	−1.67
2007	7.89	2.49	26.75	5.26	—	0.58	9.21	47.81	−0.36
2008	9.24	17.55	3.93	—	38.57	5.08	—	25.64	−1.22
2005–08	4.7	6.21	8.4	2.14	16.08	15.91	2.81	43.74	—

by clouds and precipitation processes during airmass transport along marine pathways and clear-airmass dilution over the Arctic basin. The BC time series were represented by 2–5.4- and 6–14-day atmospheric variations with long-range transport of pollutants from the LS/KS.

Further consideration of the effect of atmospheric circulation patterns on BC concentration is based on the study of BC corresponding to each cluster and the NAO index for each year. It is worth noting that when the NAO index was negative in 2005, BCA_{tr} concentrations in the BS/CS/BFS cluster were negative, while during the negative phase of NAO, BCA_{tr} concentrations were positive. For the remaining clusters, no trends seem to be present for the period of this study. While the different circulation patterns were one of the factors causing the year-to-year variation, changes in emission and deposition were also important for the measured BC concentration at the station.

4. Conclusions

Measurements of aerosol black carbon (BC) were made in the summertime from 2005 to 2008 using an aethalometer at the ''Yellow River'' Station near Ny-Ålesund in the Svalbard Islands. The background and the median BC concentrations were calculated as 7.2 and 14.6 ng m^{-3}, respectively. A net rate of increase of BC of about 4 ng m^{-3} a^{-1} was found from 2005 to 2008 at this location; BC from local emissions was mostly responsible for the observed increase.

Time series of BC are analyzed using the EEMD method. Results reveal that it includes various timescale oscillations. IMF1 and IMF2 are mostly dominated by a component with a period of about 3 and 6–12 h, which have no correlation with meteorological factors, while the correlations between IMF3 and meteorological elements were different for each year. IMF4 is mostly dominated by a component with a 1–3-day variation characterized by strong wind and usually a linkage with low pressure systems developing in the Atlantic Ocean and traveling through Europe into the Arctic. IMF5 is the frequency component of low pressure systems in Arctic basins, the European continent, and northeastern Canada. IMF6 is mostly dominated by a component with a period of 6–14 days, which implies the frequency of wave train in high latitudes and Siberian cyclonic activity. IMF7 and IMF8 are mostly dominated by a longer period of about 20 days.

The 7-day back-trajectory and cluster analysis reveals that the cluster contributing most BC to the sampling station was from the North Atlantic Ocean and northern Europe. The highest BC events over the Yellow River Station were associated with transport pathways and source regions from northern Europe.

Uncertainty remains for the relationship between the NAO and the frequency of year-to-year BC variations. Comparison of trajectories with the NAO index reveals that the frequency of trajectories from the GS/NS cluster was enhanced during the positive phase of NAO and reduced during the negative phase of NAO. At this location, a larger influence from trajectories in the SC/BS/KS and GS/NS clusters was found with more pollutants transported from northern Europe and the North Atlantic Ocean. Only a weak linkage could be found between BCA_{tr} in the BS/CS/BFS cluster and the NAO index; BCA_{tr} is higher during the negative phases than during the positive phases.

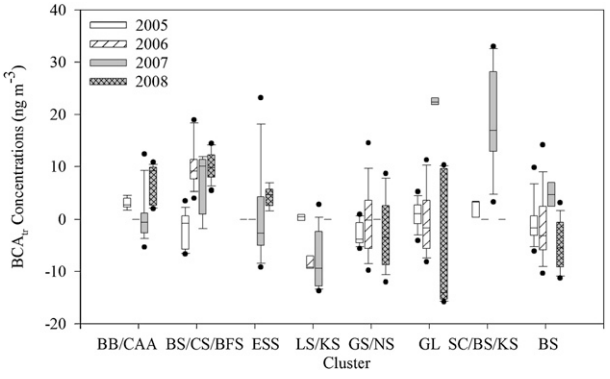

FIG. 8. Distribution of BCA_{tr} concentrations (defined as BC_{tr} minus BC_{tr} mean) for eight clusters for all the years in the summer showing the median, 5th, 25th, 75th, and 95th percentiles.

Acknowledgments. This work was funded by the National Natural Science Foundation of China (Grant 41105094); the Scientific Research Foundation of Third Institute of Oceanography, State Oceanic Administration of China (Grant 2011004); and the Chinese Projects for Investigations and Assessments of the Arctic and Antarctic (CHINARE 2012-15 for 01-04-02, 02-01, and 03-04-02). The Chinese Arctic and Antarctic Administration of State Oceanic Administration supported field accommodations at Yellow River Station. We gratefully acknowledge the U.S. National Oceanic and Atmospheric Administration's Air Resources Laboratory for providing the HYSPLIT transport and dispersion model and NCAR–NCEP for providing the meteorological data freely.

REFERENCES

Bauer, S. E., and S. Menon, 2012: Aerosol direct, indirect, semi-direct, and surface albedo effects from sector contributions based on the IPCC AR5 emissions for preindustrial and present-day conditions. *J. Geophys. Res.*, **117**, D01206, doi:10.1029/2011jd016816.

Bond, T. C., and H. L. Sun, 2005: Can reducing black carbon emissions counteract global warming? *Environ. Sci. Technol.*, **39**, 5921–5926, doi:10.1021/es0480421.

——, and Coauthors, 2013: Bounding the role of black carbon in the climate system: A scientific assessment. *J. Geophys. Res. Atmos.*, **118**, 5380–5552, doi:10.1002/jgrd.50171.

Dalsøren, S. B., M. S. Eide, Ø. Endresen, A. Mjelde, G. Gravir, and I. S. A. Isaksen, 2009: Update on emissions and environmental impacts from the international fleet of ships: The contribution from major ship types and ports. *Atmos. Chem. Phys.*, **9**, 2171–2194, doi:10.5194/acp-9-2171-2009.

Draxler, R. R., and G. D. Hess, 1998: An overview of the HYSPLIT_4 modeling system for trajectories, description, and deposition. *Aust. Meteor. Mag.*, **47**, 295–308.

Eckhardt, S., O. Hermansen, H. Grythe, M. Fiebig, K. Stebel, M. Cassiani, A. Baecklund, and A. Stohl, 2013: The influence of cruise ship emissions on air pollution in Svalbard—A harbinger of a more polluted Arctic? *Atmos. Chem. Phys.*, **13**, 8401–8409, doi:10.5194/acp-13-8401-2013.

Eleftheriadis, K., S. Vratolis, and S. Nyeki, 2009: Aerosol black carbon in the European Arctic: Measurements at Zeppelin station, Ny-Ålesund, Svalbard from 1998–2007. *Geophys. Res. Lett.*, **36**, L02809, doi:10.1029/2008GL035741.

Hansen, A. D. A., J. R. Turner, and G. A. Allen, 2007: An algorithm to compensate Aethalometer data for the effects of optical shadowing and scattering. Preprints, *Fifth Asian Aerosol Conf.*, Kaohsiung, Taiwan, Asian Aerosol Research Assembly, 119.

Heintzenberg, J., and C. Leck, 1994: Seasonal variation of the atmospheric aerosol near the top of the marine boundary layer over Spitsbergen related to the Arctic sulphur cycle. *Tellus*, **46B**, 52–67, doi:10.1034/j.1600-0889.1994.00005.x.

Hirdman, D., and Coauthors, 2010: Long-term trends of black carbon and sulphate aerosol in the Arctic: Changes in atmospheric transport and source region emissions. *Atmos. Chem. Phys.*, **10**, 9351–9368, doi:10.5194/acp-10-9351-2010.

Huang, N. E., and Z. Wu, 2008: A review on Hilbert-Huang transform: Method and its applications to geophysical studies. *Rev. Geophys.*, **46**, RG2006, doi:10.1029/2007RG000228.

——, Z. Shen, and S. R. Long, 1998: The empirical mode decomposition and the Hilbert spectrum for nonlinear and non-stationary time series analysis. *Proc. Roy. Soc. London*, **454**, 903–995, doi:10.1098/rspa.1998.0193.

——, ——, and ——, 1999: A new view of nonlinear water waves: The Hilbert spectrum. *Annu. Rev. Fluid Mech.*, **31**, 417–457, doi:10.1146/annurev.fluid.31.1.417.

IPCC, 2013: *Climate Change: The Physical Science Basis*. Cambridge University Press, 1535 pp.

Nyeki, S., H. Bauer, H. Puxbaum, C. Dye, K. Teinila, R. Hillamo, J. Ström, and K. Eleftheriadis, 2005: Comparison of black carbon concentrations derived by filter-based light transmission and thermo-optical techniques for Arctic aerosol. *Extended Abstracts*, *European Aerosol Conf.*, Ghent, Belgium, European Aerosol Assembly, 122–123.

Polissar, A. V., P. K. Hopke, P. Paatero, Y. J. Kaufmann, D. K. Hall, B. A. Bodhaine, E. G. Dutton, and J. M. Harris, 1999: The aerosol at Barrow, Alaska: Long-term trends and source locations. *Atmos. Environ.*, **33**, 2441–2458, doi:10.1016/S1352-2310(98)00423-3.

Quinn, P. K., and Coauthors, 2011: The impact of black carbon on Arctic climate. Arctic Monitoring and Assessment Programme Tech. Rep. 4, 72 pp.

Sharma, S., D. Lavoué, H. Cachier, L. A. Barrie, and S. L. Gong, 2004: Long-term trends of the black carbon concentrations in the Canadian Arctic. *J. Geophys. Res.*, **109**, D15203, doi:10.1029/2003JD004331.

——, E. Andrews, L. A. Barrie, J. A. Ogren, and D. Lavoué, 2006: Variations and sources of the equivalent black carbon in the high Arctic revealed by long-term observations at Alert and Barrow: 1989–2003. *J. Geophys. Res.*, **111**, D14208, doi:10.1029/2005JD006581.

——, M. Ishizawa, D. Chan, D. Lavoué, E. Andrews, K. Eleftheriadis, and S. Maksyutov, 2013: 16-year simulation of Arctic black carbon: Transport, source contribution, and sensitivity analysis on deposition. *J. Geophys. Res. Atmos.*, **118**, 943–964, doi:10.1029/2012JD017774.

Stohl, A., Z. Klimont, S. Eckhardt, K. Kupiainen, V. P. Shevchenko, V. M. Kopeikin, and A. N. Novigatsky, 2013: Black carbon in the Arctic: The underestimated role of gas flaring and residential combustion emissions. *Atmos. Chem. Phys.*, **13**, 8833–8855, doi:10.5194/acp-13-8833-2013.

Vestreng, V., E. Økstad, and R. Kallenborn, 2009: Climate influencing emissions, scenarios and mitigation options at Svalbard. Klif Rep TA-2552, 52 pp. [Available online at http://www.miljodirektoratet.no/old/klif/publikasjoner/2552/ta2552.pdf.]

Wu, Z. H., and N. E. Huang, 2009: Ensemble empirical mode decomposition: A noise-assisted data analysis method. *Adv. Adapt. Data Anal.*, **1**, 1–41, doi:10.1142/S1793536909000047.

Zhan, J., and Y. Gao, 2014: Impact of summertime anthropogenic emissions on atmospheric black carbon at Ny-Åesund in the Arctic. *Polar Res.*, **33**, 21821, doi:10.3402/polar.v33.21821.

——, ——, W. Li, L. Chen, H. Lin, and Qi Lin, 2014: Effects of ship emissions on summertime aerosols at Ny-Ålesund in the Arctic. *Atmos. Pollut. Res.*, **5**, 500–510, doi:10.5094/APR.2014.059.